

in the theory (for one extra dimension). For the ADD theory with two large extra compact dimensions, we do not quite reach the limit on the size of these dimensions already set in refs 11 and 12.

Besides forces from extra dimensions, two other ideas have suggested new weak forces at submillimetre scales. The cosmological energy density needed to close the universe, if converted to a length by taking its inverse fourth root (in natural units where $\hbar = c = 1$), corresponds to about $100\text{ }\mu\text{m}$. This fact has led to repeated attempts^{17–19} to address difficulties connected with the very small observed size of Einstein's cosmological constant by introducing new forces with a range near $100\text{ }\mu\text{m}$. Our result is the best upper bound on α in this region, but we have not quite reached gravitational sensitivity. Finally, the oldest of these predictions, still out of reach, is the very feeble axion-mediated force^{20,21}. The axion is a field intended to explain why the violation of charge-parity symmetry is so small in quantum chromodynamics, the theory of the strong nuclear force.

Experiments of the sort reported here constrain string-inspired scenarios by setting very restrictive limits on predicted submillimetre forces. Of course, the actual observation of any new force would be a major advance. Because several theoretical scenarios point especially to these length scales, it is an important goal for the future to reach gravitational strength at even shorter distances, perhaps down to $10\text{ }\mu\text{m}$. Experiments attempting to reach such distances will confront rapidly increasing background forces, especially electrostatic forces arising from the spatially non-uniform surface potentials of metals²². Electric fields due to surface potentials can be shielded with good conductors, but because of the finite stiffness of any shield they still cause background forces to be transmitted between test masses. Stretched membranes (as used by the Washington group) are more effective than stiff plates at the shortest distances, but it remains to be seen down to what distance the background forces can be effectively suppressed. \square

Received 21 October 2002; accepted 13 January 2003; doi:10.1038/nature01432.

1. Greene, B. *The Elegant Universe: Superstrings, Hidden Dimensions, and the Quest for the Ultimate Theory* (Norton, New York, 1999).
2. Kaplan, D. B. & Wise, M. B. Couplings of a light dilaton and violations of the equivalence principle. *J. High Energy Phys.* **8**, 37 (2000).
3. Taylor, T. R. & Veneziano, G. Dilaton couplings at large distances. *Phys. Lett. B* **213**, 450–454 (1988).
4. Dimopoulos, S. & Giudice, G. Macroscopic forces from supersymmetry. *Phys. Lett. B* **379**, 105–114 (1996).
5. Antoniadis, I. A possible new dimension at a few TeV. *Phys. Lett. B* **246**, 377–384 (1990).
6. Antoniadis, I., Dimopoulos, S. & Dvali, G. Millimeter-range forces in superstring theories with weak-scale compactification. *Nucl. Phys. B* **516**, 70–82 (1998).
7. Chacko, Z. & Perazzi, E. Extra dimensions at the weak scale and deviations from Newtonian gravity. Preprint hep-ph/0210254 available at (arXiv.org) (2002).
8. Fischbach, E. & Talmadge, C. *The Search for Non-Newtonian Gravity* (Springer, New York, 1999).
9. Bordag, M., Mohideen, U. & Mostepanenko, V. M. New Developments in the Casimir effect. *Phys. Rep.* **353**, 1–205 (2001).
10. Long, J. C., Chan, H. W. & Price, J. C. Experimental status of gravitational-strength forces in the sub-centimeter regime. *Nucl. Phys. B* **539**, 23–34 (1999).
11. Hoyle, C. D. et al. Sub-millimeter tests of the gravitational inverse-square law: A search for “large” extra dimensions. *Phys. Rev. Lett.* **86**, 1418–1421 (2001).
12. Adelberger, E. G. Sub-mm tests of the gravitational inverse-square law. Preprint hep-ex/0202008 available at (arXiv.org) (2002).
13. Fischbach, E., Krause, D. E., Mostepanenko, V. M. & Novello, M. New constraints on ultrashort-ranged Yukawa interactions from atomic force microscopy. *Phys. Rev. D* **64**, 075010 (2001).
14. Arkani-Hamed, N., Dimopoulos, S. & Dvali, G. The hierarchy problem and new dimensions at a millimeter. *Phys. Lett. B* **429**, 263–272 (1998).
15. Kleiman, R. N., Kaminsky, G. K., Reppy, J. D., Pindak, R. & Bishop, D. J. Single-crystal silicon high-Q torsional oscillators. *Rev. Sci. Instrum.* **56**, 2088–2091 (1985).
16. Long, J. C. et al. New experimental limits on macroscopic forces below 100 microns. Preprint hep-ph/0210004 available at (arXiv.org) (2002).
17. Beane, S. R. On the importance of testing gravity at distances less than 1 cm. *Gen. Rel. Grav.* **29**, 945–951 (1997).
18. Sundrum, R. Towards an effective particle-string resolution of the cosmological constant problem. *J. High Energy Phys.* **7**, 1 (1999).
19. Schmidhuber, C. Old puzzles. Preprint hep-th/0207203 available at (arXiv.org) (2002).
20. Moody, J. E. & Wilczek, F. New macroscopic forces? *Phys. Rev. D* **30**, 130–138 (1984).
21. Rosenberg, L. J. & van Bibber, K. A. Searches for invisible axions. *Phys. Rep.* **325**, 1–39 (2000).
22. Price, J. C. in *Proc. Int. Symp. on Experimental Gravitational Physics* (eds Michelson, P., En-ke, H. & Pizzella, G.) 436–439 (World Scientific, Singapore, 1988).
23. Chan, H. W., Long, J. C. & Price, J. C. Taber vibration isolator for vacuum and cryogenic applications. *Rev. Sci. Instrum.* **70**, 2742–2750 (1999).

24. Lamoreaux, S. K. Demonstration of the Casimir force in the 0.6 to $6\text{ }\mu\text{m}$ range. *Phys. Rev. Lett.* **78**, 5–8 (1997).
25. Hoskins, J. K., Newman, R. D., Spero, R. & Shultz, J. Experimental tests of the gravitational inverse-square law for mass separations from 2 to 105 cm . *Phys. Rev. D* **32**, 3084–3095 (1985).
26. Chiaverini, J., Smullin, S. J., Geraci, A. A., Weld, D. M. & Kapitulnik, A. New experimental constraints on non-Newtonian forces below 100 microns. Preprint hep-ph/0209325 available at (arXiv.org) (2002).
27. Floratos, E. G. & Leontaris, G. K. Low scale unification, Newton's law and extra dimensions. *Phys. Lett. B* **465**, 95–100 (1999).
28. Kehagias, A. & Sfetsos, K. Deviations from the $1/r^2$ Newton law due to extra dimensions. *Phys. Lett. B* **472**, 39–44 (2000).

Acknowledgements We thank E. Lagae for work in the laboratory, and C. Briggs, T. Buxkemper, L. Czaia, H. Green, S. Gustafson and H. Rohner of the University of Colorado and JILA instrument shops for technical assistance. We also gratefully acknowledge discussions with S. de Alwis, B. Dobrescu and S. Dimopoulos. This work is supported by grants from the US National Science Foundation.

Competing interests statement The authors declare that they have no competing financial interests.

Correspondence and requests for materials should be addressed to J.C.P. (e-mail: john.price@colorado.edu).

Ultra-high-*Q* toroid microcavity on a chip

D. K. Armani, T. J. Kippenberg, S. M. Spillane & K. J. Vahala

Department of Applied Physics, California Institute of Technology, Pasadena, California 91125, USA

The circulation of light within dielectric volumes enables storage of optical power near specific resonant frequencies and is important in a wide range of fields including cavity quantum electrodynamics^{1,2}, photonics^{3,4}, biosensing^{5,6} and nonlinear optics^{7–9}. Optical trajectories occur near the interface of the volume with its surroundings, making their performance strongly dependent upon interface quality. With a nearly atomic-scale surface finish, surface-tension-induced microcavities such as liquid droplets or spheres^{10–13} are superior to all other dielectric microresonant structures when comparing photon lifetime or, equivalently, cavity *Q* factor. Despite these advantageous properties, the physical characteristics of such systems are not easily controlled during fabrication. It is known that wafer-based processing¹⁴ of resonators can achieve parallel processing and control, as well as integration with other functions. However, such resonators-on-a-chip suffer from *Q* factors that are many orders of magnitude lower than for surface-tension-induced microcavities, making them unsuitable for ultra-high-*Q* experiments. Here we demonstrate a process for producing silica toroid-shaped microresonators-on-a-chip with *Q* factors in excess of 100 million using a combination of lithography, dry etching and a selective reflow process. Such a high *Q* value was previously attainable only by droplets or microspheres and represents an improvement of nearly four orders of magnitude over previous chip-based resonators.

Devices were fabricated upon silicon wafers prepared with a $2\text{-}\mu\text{m}$ layer of silicon dioxide (SiO_2). The fabrication process flow is composed of four steps: photolithography; pattern transfer into the silicon dioxide layer; selective, dry etch of the exposed silicon; and selective reflow of the patterned silica. The process details are as follows (Fig. 1). First, photolithography is performed to create disk-shaped photo-resist pads (160 μm in diameter) on a (100) prime grade silicon substrate with 2 μm of oxide grown using wet thermal oxidation in a horizontal tube furnace. An additional bake follows in order to reflow the photo-resist, smoothing the edges in the

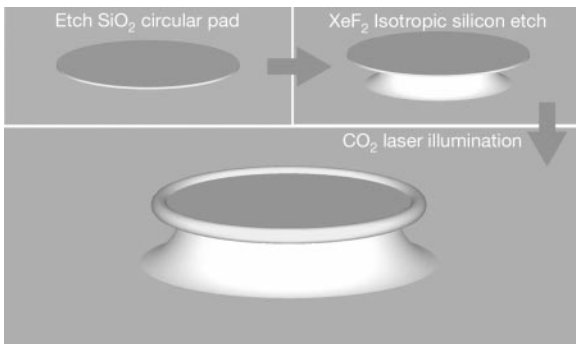


Figure 1 Flow diagram illustrating the process used to fabricate ultra-high-*Q* planar microcavities.

process. The circular disks of photo-resist act as an etch mask during immersion in buffered HF solution at room temperature. Acetone is then used to remove residual photo-resist and organic contamination. The remaining SiO_2 disks act as etch masks during exposure to XeF_2 gas at 3 torr. XeF_2 was specifically chosen for the purpose of isotropic selective removal of silicon. As a result, the edges of the SiO_2 disks are equally undercut, leaving circular silicon pillars supporting larger SiO_2 disks. As the optical trajectories of interest reside at the periphery of the silica disk, the removal of the higher-index silicon below a portion of the periphery is required to inhibit power leakage into the substrate. We observe *Q* values in excess of 10^5 for these structures using the spectral characterization approach described below. The above process flow leaves lithographic blemishes, visible in an optical microscope, at the all-important disk periphery. Therefore we used additional processing to achieve the surface finish characteristic of surface-tension-induced microcavity structures (root-mean-square (r.m.s) roughness of several nanometres or less¹³).

Next, a processing step is introduced to selectively heat and reflow the undercut SiO_2 disks without affecting the underlying silicon support pillar. An undercut SiO_2 disk is surface-normal-irradiated using a CO_2 laser (10.6- μm wavelength), similar to techniques proposed for integrated circuit planarization¹⁵. The beam intensity profile follows an approximately gaussian distribution and is focused to a circular spot approximately 200 μm in diameter. The resulting beam intensity can be varied by electronic control of the laser power, but is typically 100 MW m^{-2} during reflow. Owing to the strong temperature dependence of the silica optical extinction coefficient near 10.6 μm (ref. 16) as well as the thermal isolation of the undercut SiO_2 disk, melting of the disk occurs along the periphery, and significantly not over the silicon pillar. In addition to having a far weaker optical absorption at 10.6 μm , silicon is 100 times more thermally conductive than silica^{16,17}. The silicon pillar therefore remains significantly cooler and physically unaffected throughout the silica reflow process, serving as a heat sink to the selectively absorbed optical power in the silica layer. As the disk diameter shrinks, the effective cross-section available to absorb laser power decreases and shrinkage is observed to terminate when a toroid-like silica structure has formed. Beyond this point, continued laser treatment at the same intensity results in no observable change of the structure. The process is therefore self-quenching with the final diameter of the molten disk rim controlled by lithography and chemical etch steps. It should be noted that it is possible to interrupt the reflow prior to quenching thereby producing a toroid with a diameter intermediate to the initial disk diameter and terminal diameter.

Thus, in this process step, surface tension both smoothes the surface and collapses the silica disk to a toroid shape with limiting dimensions defined by the support pillar and the initial thickness of the silica layer. Micrographs showing disks both before and after the

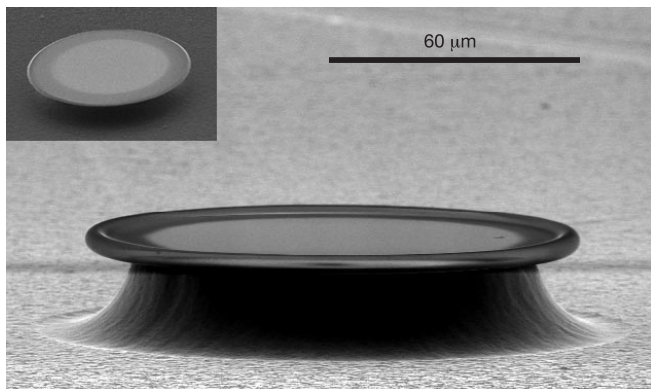


Figure 2 Scanning electron micrograph of a silica microdisk after selective reflow treatment with a CO_2 laser. The inset shows the microdisk prior to laser treatment. This toroidal microresonator had an intrinsic cavity *Q* of 1.00×10^8 .

laser-activated selective reflow process are shown in Fig. 2. In these micrographs, the overall disk diameter was reduced to 120 μm as silica was consumed to form a 7- μm -thick toroid-shaped perimeter.

The mode structure and quality factor of the toroidal cavities were characterized in the optical telecommunication band (1,500 nm wavelength band). Tapered optical fibres connected to a single-mode, tunable, external-cavity laser were used to efficiently excite ‘whispering gallery’ modes of the resonators. Tapered waveguides were positioned on a 20-nm-resolution stage and could be moved freely over the silicon sample to couple individually to each of the toroid-shaped microresonators. Dual microscopes were used to simultaneously image disk resonators and fibre tapers from the side and the top. Proper alignment required the taper axis to reside in the equatorial plane of the toroidal cavity with minimal tilt angle. Briefly, taper fabrication¹⁸ proceeds by stretching a standard optical fibre (SMF-28), which has been heated using a hydrogen flame. By observing the adiabatic condition, the tapered fibers exhibit low fibre-to-fibre insertion loss (typically <10%). Taper waist diameters are typically several micrometres, adjusted to properly phase-match to the resonator. Critical coupling¹⁹ (the resonant transfer of all optical waveguide power into the resonator) was achieved by appropriately adjusting the taper–resonator gap. Non-resonant loss was observed to be low (<5%).

Figure 3 shows the transmission spectra through a taper in close proximity (of the order of hundreds of nanometres) to a 94- μm -diameter toroidal microresonator. The observed free spectral range corresponds to the equatorial mode number (*l*-index). Inspection of the data shows that the resonator supports very few radial and azimuthal (*m*-index or transverse) modes. This is in contrast to spheres, which support $(2l + 1)$ azimuthal modes. The quality factor, or *Q*, of the resonators was measured in two ways. First, the full-width at half-maximum (FWHM) of the lorentzian-shaped resonance in the undercoupled regime was directly measured by scanning a single-mode laser (short-term linewidth about 300 kHz) through a resonance. Low input power levels (typically less than 5 μW) were used to avoid thermally induced distortion of the line shape caused by resonant-field build-up within the cavity. Repeated measurements on samples fabricated with various radii (80–120 μm) and tori thickness (5–10 μm) yielded *Q* values in excess of 100 million (10^8). This is a record value for a planar device, and constitutes an improvement of nearly four orders of magnitude over all previous planar microresonators fabricated by wafer-scale processing (the highest values^{20,21} reported thus far are less than 2×10^4).

As an independent and more precise measurement of quality factor, the photon lifetime was directly measured by cavity ring-down. This was done by repeatedly scanning the laser into resonance with a mode that was critically coupled to the taper. As the laser

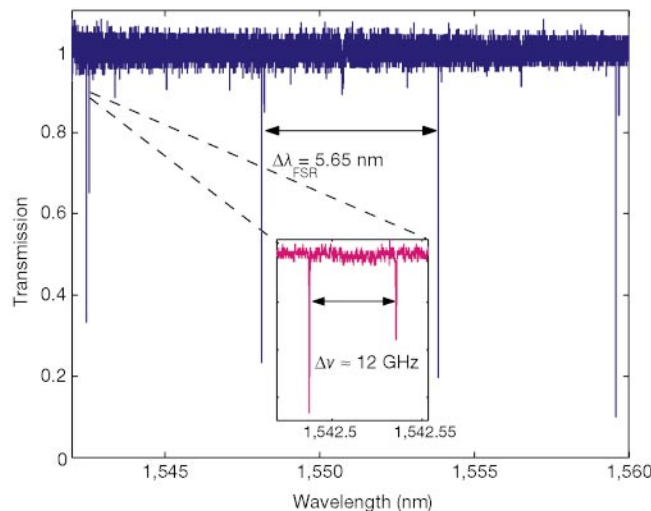


Figure 3 Transmission spectra of a toroidal resonator. The free spectral range (defined as the wavelength spacing between modes with successive angular mode number) is 5.65 nm, which corresponds to a torus approximately 94 μm in diameter. The inset shows what we believe to be the two lowest-order radial modes (based on modelling of a microdisk resonator). Additional subsidiary peaks are attributed to other radial or azimuthal modes.

scanned into resonance, power transfer increased until maximal ‘charging’ of the resonant mode was attained. At this moment, the laser input was gated ‘off’ by use of a high-speed, external modulator and cavity ringdown is observed as the resonant power discharges. Because the resonator is by necessity loaded during this measurement, the observed ringdown time yields the cavity lifetime at the critical point, τ_{crit} , and the loaded Q-factor (not the intrinsic quality factor, Q_0). Data from a typical ringdown measurement are shown in Fig. 4. At time $t = 0$ in the figure, a signal is applied to ‘gate’ the laser off. When the laser input is fully off, the detected power is due entirely to the cavity discharge field. The solid line represents an exponential fit as expected for decay of a single cavity mode. The inset shows a logarithmic plot to infer the cavity lifetime. The loaded lifetime in this structure was 43 ns. As a further check on this time constant, after gating of the pump laser the waveguide power has dropped to 80% of its predicted maximal value based on extrapolation of data to $t = 0$. This value is in agreement with the gating delay of the ringdown setup ($\Delta t \approx 8$ ns). In particular, using the observed mode-lifetime of $\tau_{\text{crit}} = 43$ ns yields $\exp(-\Delta t/\tau_{\text{crit}}) = 0.83$.

As noted before, to infer the intrinsic cavity Q it is necessary to correct for loading by the taper waveguide. In addition, it is necessary to take into account excitation of the counter-propagating mode due to scattering centres intrinsic to the resonator (described by a dimensionless intermode coupling parameter Γ). The techniques used to measure this parameter in ultra-high-Q taper-coupled resonators are described elsewhere²². For the mode of Fig. 4 the intermode coupling was measured to be approximately 1, giving rise to a weak counter-propagating wave excitation (17% of the cavity build-up field is stored in the counter-propagating mode at critical coupling). In the presence of intermode coupling the relationship between the critically coupled lifetime and the intrinsic (unloaded) cavity quality factor, is given by

$$Q_0 \equiv \omega\tau_0 = \omega\tau_{\text{crit}}(1 + \sqrt{1 + \Gamma^2})$$

This yields an intrinsic cavity Q of 1.25×10^8 inferred from cavity ringdown. This value agrees with the measurements of the frequency line shape described above.

Thus we have fabricated ultra-high-Q planar cavities on a chip for the first time (to our knowledge). Toroid-shaped microcavities were

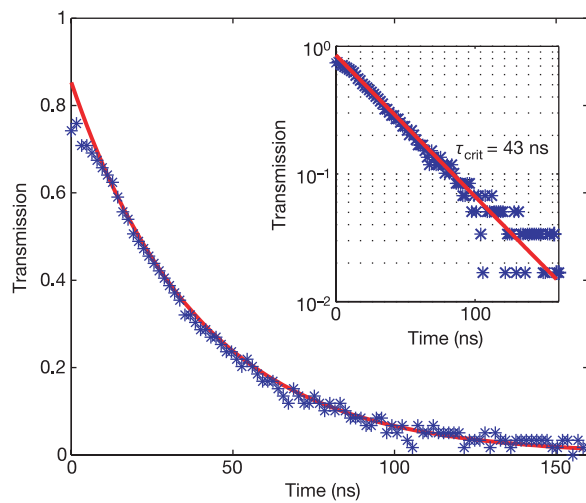


Figure 4 Ringdown measurement of a 90- μm -diameter toroid microcavity at the critical-coupling point. The measured lifetime of $\tau_{\text{crit}} = 43$ ns corresponds to an intrinsic quality factor of $Q = 1.25 \times 10^8$.

formed using a combination of lithography, dry etching and a selective reflow process. Self-limited collapse of a molten silica disk enables the dimensional control typical of wafer-scale processing while providing the surface finish (and hence cavity Q) typical of a spherical resonator. Q values obtained by this process are typically four orders of magnitude higher than previous wafer-based resonators. In some applications mode volume is also an important factor, and certain chip-based micro-resonators^{20,21} feature smaller mode volumes than the present structures. As a gauge to the lower bound on size, radiation leakage becomes a significant factor in determining Q for diameters less than 20 μm in silica microspheres. It should therefore be possible to reduce toroid diameter (and hence mode volume) substantially from the present 100 μm while maintaining ultra-high- Q values. The planar nature of the toroid microcavity and the large transparency window of silica suggest that these devices will find a wide range of applications in photonics as well as in fundamental studies. As an indication of the possibilities for these structures, in the course of this work nonlinear optical effects have been observed with characteristics comparable to recent studies on spherical ultra-high- Q cavities⁹. As standard processing techniques are used, the addition of optical functionality by techniques such as implantation or coating is possible. Likewise, electrical functionality can be introduced to integrate control functions with the ultra-high- Q microcavities. More generally, this work provides a new functional element that is synergistic with recent demonstrations of basic experimental physics on a chip. For example, by combining the present results with techniques recently demonstrated to integrate atomic traps on a chip²³ it would be possible to achieve chip-scale integration of cavity quantum electrodynamics experiments and related devices. Finally, there is great interest in improving the sensitivity of biological and chemical sensors. Proposals based upon optical resonators will benefit from the ability to attain ultra-high Q on a chip. □

Received 10 October; accepted 16 December 2002; doi:10.1038/nature01371.

1. Lefevre-Seguin, V. & Haroche, S. Towards cavity-QED experiments with silica microspheres. *Mater. Sci. Eng. B* **48**, 53–58 (1997).
2. Vernooy, D. W., Furusawa, A., Georgiades, N. P., Ilchenko, V. S. & Kimble, H. J. Cavity QED with high-Q whispering gallery modes. *Phys. Rev. A* **57**, R2293–R2296 (1998).
3. McCall, S. L., Levi, A. F. J., Slusher, R. E., Pearton, S. J. & Logan, R. A. Whispering-gallery mode microdisk lasers. *Appl. Phys. Lett.* **60**, 289–291 (1992).
4. Sandoghdar, V. *et al.* Very low threshold whispering-gallery-mode microsphere laser. *Phys. Rev. A* **54**, R1777–R1780 (1996).
5. Vollmer, F. *et al.* Protein detection by optical shift of a resonant microcavity. *Appl. Phys. Lett.* **80**, 4057–4059 (2002).

6. Serpenguzel, A., Arnold, S. & Griffel, G. Excitation of resonances of microspheres on an optical fiber. *Opt. Lett.* **20**, 654–656 (1995).
7. Chang, R. K. & Campillo, A. J. (eds) *Optical Processes in Microcavities* (World Scientific, Singapore, 1996).
8. Treussart, F. et al. Evidence for intrinsic Kerr bistability of high-Q microsphere resonators in superfluid helium. *Eur. Phys. J. D* **1**, 235–238 (1998).
9. Spillane, S. M., Kippenberg, T. J. & Vahala, K. J. Ultralow-threshold Raman laser using a spherical dielectric microcavity. *Nature* **415**, 621–623 (2002).
10. Campillo, A. J., Eversole, J. D. & Lin, H.-B. Cavity quantum electrodynamic enhancement of stimulated emission in microdroplets. *Phys. Rev. Lett.* **67**, 437–440 (1991).
11. Braginsky, V. B., Gorodetsky, M. L. & Ilchenko, V. S. Quality-factor and nonlinear properties of optical whispering-gallery modes. *Phys. Lett. A* **137**, 393–397 (1989).
12. Collot, L., Lefevre-Seguin, V., Brune, M., Raimond, J. M. & Haroche, S. Very high-Q whispering-gallery mode resonances observed on fused-silica microspheres. *Europhys. Lett.* **23**, 327–334 (1993).
13. Vernooy, D. W., Ilchenko, V. S., Mabuchi, H., Steed, E. W. & Kimble, H. J. High-Q measurements of fused-silica microspheres in the near infrared. *Opt. Lett.* **23**, 247–249 (1998).
14. Himeno, A., Kato, K. & Miya, T. Silica-based planar lightwave circuits. *IEEE J. Sel. Top. Quant.* **4**, 913–924 (1998).
15. Delfino, M. & Reifsteck, T. A. Laser activated flow of phosphosilicate glass in integrated circuit devices. *Elect. Device Lett.* **3**, 116–118 (1982).
16. McLachlan, A. D. & Meyer, F. P. Temperature dependence of the extinction coefficient of fused silica for CO₂ laser wavelengths. *Appl. Opt.* **26**, 1728–1731 (1987).
17. Sheik-bahae, M. & Kwok, H. S. Controlled CO₂ laser melting of silicon. *J. Appl. Phys.* **63**, 518–524 (1988).
18. Knight, J. C., Cheung, G., Jacques, F. & Birks, T. A. Phase-matched excitation of whispering-gallery-mode resonances by a fiber taper. *Opt. Lett.* **22**, 1129–1131 (1997).
19. Cai, M., Painter, O. & Vahala, K. J. Observation of critical coupling in a fiber taper to a silica-microsphere whispering-gallery mode system. *Phys. Rev. Lett.* **85**, 74–77 (2000).
20. Michler, P. et al. Laser emission from quantum dots in microdisk structures. *Appl. Phys. Lett.* **77**, 184–186 (2001).
21. Gayral, B. et al. High-Q wet-etched GaAs microdisks containing InAs quantum boxes. *Appl. Phys. Lett.* **75**, 1908–1910 (1999).
22. Kippenberg, T. J., Spillane, S. M. & Vahala, K. J. Modal coupling in traveling-wave resonators. *Opt. Lett.* **27**, 1669–1671 (2002).
23. Hansel, W., Hommelhoff, P., Hansch, T. W. & Reichel, J. Bose-Einstein condensation on a microelectronic chip. *Nature* **413**, 498–501 (2001).

Acknowledgements This work was supported by DARPA and the Caltech Lee Center.

Competing interests statement The authors declare that they have no competing financial interests.

Correspondence and requests for materials should be addressed to K.J.V. (e-mail: vahala@caltech.edu).

Logarithmic rate dependence of force networks in sheared granular materials

R. R. Hartley & R. P. Behringer

Department of Physics & Center for Nonlinear and Complex Systems, Duke University, Durham, North Carolina 27708-0305, USA

Many models of slow, dense granular flows^{1–5} assume that the internal stresses are independent of the shearing rate. In contrast, logarithmic rate dependence is found in solid-on-solid friction^{6–8}, geological settings^{9–11} and elsewhere^{12–15}. Here we investigate the rate dependence of stress in a slowly sheared two-dimensional system of photoelastic disks, in which we are able to determine forces on the granular scale. We find that the mean (time-averaged) stress displays a logarithmic dependence on the shear rate for plastic (irreversible) deformations. However, there is no perceivable dependence on the driving rate for elastic (reversible) deformations, such as those that occur under moderate repetitive compression. Increasing the shearing rate leads to an increase in the strength of the force network and stress fluctuations. Qualitatively, this behaviour resembles the changes associated with an increase in density. Increases in the shearing rate also lead to qualitative changes in the distributions of stress build-up and relaxation events. If shearing is suddenly stopped, stress

relaxations occur with a logarithmic functional form over long timescales. This slow collective relaxation of the stress network provides a mechanism for rate-dependent strengthening.

Slow granular flows are typically described in the context of Mohr–Coulomb friction models² that resemble those used for describing friction between two solid bodies¹⁶. In the well-known solid friction scheme^{17,18}, an object on a frictional surface will resist a force and remain at rest, provided that the magnitude of the tangential force is less than the product of a static friction coefficient and the normal force. This picture was translated into the granular context (for dense granular systems characterized by networks of force chains¹⁹) by Coulomb²⁰ and more recent authors^{1,2}. In this context the normal and tangential forces are replaced by corresponding normal and shear stresses, and the surface of interaction is replaced by a plane within the material. For large enough tangential force relative to the normal force sliding friction (failure in a granular material) occurs. In these pictures, sliding friction (deformation following failure) is independent of the speed of sliding (the shear rate).

In reality, experiments in diverse contexts have shown that solid friction exhibits a logarithmic dependence on rate and that static frictional contacts strengthen logarithmically with age. These experiments span a vast range of lengths, and include studies at the atomic¹⁵, laboratory^{7,8,12–14} and geological scale^{9–11}. Recent experiments⁶ using granular materials sliding against the interior wall of a piston showed a clear rate dependence that was associated with ageing effects of individual solid-friction contacts and with the force network. Experiments^{7,8} in which a solid rough surface was pushed across a granular bed showed a slow strengthening (or ageing) with time of the (quasi-static) force, and creep before slip events. Other experiments¹¹ have found strengthening due to ageing for granular samples under large compressions. In the present experiments, which consider the grains and the force network, we show that there is a logarithmic rate-dependence in slowly sheared granular materials that is associated with irreversible rearrangements of the force network within the material itself. This is manifested as a strengthening with rate.

The experiments described here were carried out with a two-dimensional realization of a granular system. The particles were made of a photoelastic material, and were either relatively thin disks or flat particles with a pentagonal cross-section. By using a photoelastic material, we could determine forces at the grain scale. More detailed descriptions of the experimental apparatus and methods²¹

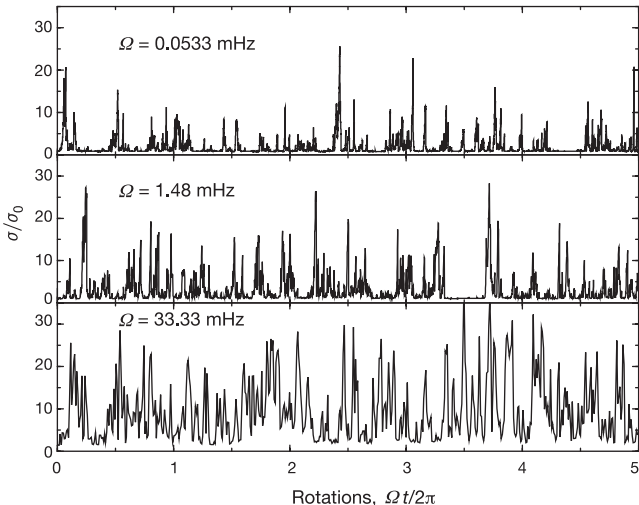


Figure 1 Time series for stress (normalized by $\sigma_0 \approx 4.11 \text{ N m}^{-1}$) for a range of shearing rates Ω that span the experimental range. These data are for pentagonal particles, but data for disks are qualitatively similar. Shear wheel radius 13.8 cm, $\gamma = \gamma_c + 0.0152$.